
[View Journal Online](#)  
[View Article Online](#)

# Synthesis, crystal structure, DFT studies, and Hirshfeld surface analysis of 2,2'-(((methylene-bis(4,1-phenylene))bis(azanylylidene))bis(methanylylidene))diphenol

 Goutam Kumar Patra <sup>1,\*</sup> and Dinesh De <sup>2</sup>
<sup>1</sup> Department of Chemistry, Faculty of Physical Sciences, Guru Ghasidas Vishwavidyalaya, Bilaspur, Chhattisgarh, 495009, India

<sup>2</sup> Department of Basic Science, Vishwavidyalaya Engineering College, Ambikapur, CSVTU-Bhilai, Chhattisgarh, 497001, India

 \* Corresponding author at: Department of Chemistry, Faculty of Physical Sciences, Guru Ghasidas Vishwavidyalaya, Bilaspur, Chhattisgarh, 495009, India.  
 e-mail: [goutam.patra@ggu.ac.in](mailto:goutam.patra@ggu.ac.in) (G.K. Patra).

## RESEARCH ARTICLE

## ABSTRACT



doi 10.5155/eurjchem.13.1.49-55.2175

Received: 07 August 2021

Received in revised form: 09 October 2021

Accepted: 01 November 2021

Published online: 31 March 2022

Printed: 31 March 2022

## KEYWORDS

 H-bonding  
 Di-Schiff base  
 X-ray crystal structure  
 Density functional theory  
 Hirshfeld surface analysis  
 Molecular electrostatic potential

The synthesis, characterization, and theoretical studies of the title compound has been reported in this study. The molecular structure has been characterized by room-temperature single-crystal X-ray diffraction study which reveals that it has an angular shape with intramolecular and intermolecular hydrogen bonding. Crystal data for the title compound,  $C_{27}H_{22}N_2O_2$  ( $M = 406.46$  g/mol): monoclinic, space group  $C2/c$  (no. 15),  $a = 36.371(10)$  Å,  $b = 4.6031(12)$  Å,  $c = 12.192(3)$  Å,  $\beta = 94.972(6)^\circ$ ,  $V = 2033.5(9)$  Å<sup>3</sup>,  $Z = 4$ ,  $T = 100$  K,  $\mu(\text{MoK}\alpha) = 0.084$  mm<sup>-1</sup>,  $D_{\text{calc}} = 1.328$  g/cm<sup>3</sup>, 8812 reflections measured ( $2.248^\circ \leq 2\theta \leq 49.734^\circ$ ), 1773 unique ( $R_{\text{int}} = 0.0323$ ,  $R_{\text{sigma}} = 0.0239$ ) which were used in all calculations. The final  $R_1$  was 0.0411 ( $I > 2\sigma(I)$ ) and  $wR_2$  was 0.1165 (all data). In crystal structure, the molecule exists in the *enol* form and is located on a two-fold axis of symmetry; where the central methylene carbon atom of the diphenylmethane moiety is displaced from the aromatic ring planes. The Hirshfeld surface analysis of the title compound shows that H...H, C...H, and O...H interactions of 53.3, 13.2, and 5.4%; respectively, which exposed that the main intermolecular interactions were H...H intermolecular interactions. The HOMO-LUMO energy gap in the title compound is 2.9639 eV. Molecular electrostatic potential of the investigated compound has also been studied.

 Cite this: *Eur. J. Chem.* 2022, 13(1), 49-55

 Journal website: [www.eurjchem.com](http://www.eurjchem.com)

## 1. Introduction

Compounds containing imine group ( $-\text{CH}=\text{N}-$ ) are known as Schiff bases and are usually prepared by condensing primary amines with active carbonyl compounds, in di-Schiff base there are two units of imine group [1-3]. They are versatile and flexible ligands for forming multinuclear transition metal complexes with interesting properties *viz.* reversible oxygen-binding ability and catalysis for several reactions [4-7]. The predilection and adaptability of imine functionality can be endorsed to its effortless synthesis, stability towards hydrolysis, and most prominently the flexible nature of  $-\text{N}=\text{CH}-$  bonds through tautomerism, which facilitate its incorporation in different applications [8,9]. Bis-bidentate Schiff base ligands have also attracted significant interest as building blocks in metallo-supramolecular chemistry, especially in the synthesis of helicate [10-13]. Free N-salicylideneanilines are often thermochromic due to a temperature-dependent equilibrium between the *keto*-amine and *enol*-imino form [14,15].

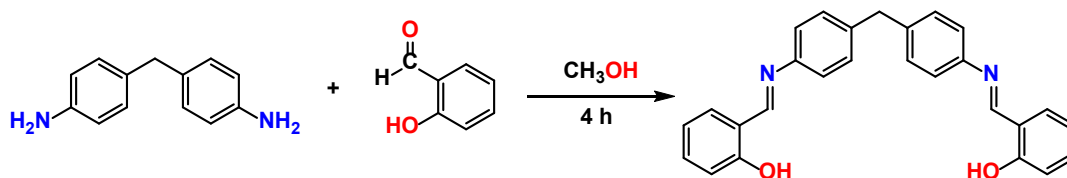
Schiff bases with *ortho*-substituted aromatic rings have found to be most responsive for chelation with transition metal ions. The chelation of transition metal ions to the  $>\text{C}=\text{N}$  linkage would develop intramolecular charge transfer (ICT) transition

or make ligand to metal charge transfer (LMCT) transition, which could be useful for the visual sensing of the metal ions [16-18]. In this regard, 4-(diethylamino)-2-hydroxybenzaldehyde is a well-known chromophore used in the area of chemosensors. Similar type of *bis*-N,O-bidentate Schiff-base ligands can be electronically and configurationally controlled, leading to a systematic study of the self-assembly process in solution [19].

In continuation to our previous research work for the search potential important functionalized *bis*-Schiff [20-22], we report here the synthesis, crystal structure, DFT studies, and Hirshfeld surface analysis of a multidentate *bis*-Schiff base, 2,2'-(((methylene-bis(4,1-phenylene))bis(azanylylidene))bis(methanylylidene))diphenol (**1**), 1+2 condensate of 4-(4-aminobenzyl)benzenamine and 2-hydroxybenzaldehyde. For designing *bis*-Schiff base compound **1**, we have selected amine part using two aniline moieties joined through a methylene rotor at their *para* positions and aldehyde part containing strong electron donating hydroxyl group also in *ortho* position to the aldehyde, which makes it electron rich [23,24].

**Table 1.** Crystal data and structure refinement parameters for the title compound **1**.

Empirical formula	C <sub>27</sub> H <sub>22</sub> N <sub>2</sub> O <sub>2</sub>
Formula weight	406.46
Temperature (K)	100
Crystal system	Monoclinic
Space group	C2/c
a, (Å)	36.371(10)
b, (Å)	4.6031(12)
c, (Å)	12.192(3)
α (°)	90
β (°)	94.972(6)
γ (°)	90
Volume (Å <sup>3</sup> )	2033.5(9)
Z	4
ρ <sub>calc</sub> (g/cm <sup>3</sup> )	1.328
μ (mm <sup>-1</sup> )	0.084
F(000)	856.0
Crystal size (mm <sup>3</sup> )	0.22 × 0.21 × 0.18
Radiation	MoKα (λ = 0.71073)
2θ range for data collection (°)	2.248 to 49.734
Index ranges	-42 ≤ h ≤ 42, -5 ≤ k ≤ 5, -14 ≤ l ≤ 14
Reflections collected	8812
Independent reflections	1773 [R <sub>int</sub> = 0.0323, R <sub>sigma</sub> = 0.0239]
Data/restraints/parameters	1773/0/146
Goodness-of-fit on F <sup>2</sup>	1.038
Final R indexes [I ≥ 2σ (I)]	R <sub>1</sub> = 0.0411, wR <sub>2</sub> = 0.1063
Final R indexes [all data]	R <sub>1</sub> = 0.0561, wR <sub>2</sub> = 0.1165
Largest diff. peak/hole (e.Å <sup>-3</sup> )	0.12/-0.15

**Scheme 1.** Synthesis of compound **1**.

## 2. Experimental

### 2.1. Materials and physical measurements

All chemicals used in this study were purchased from Aldrich Chemical Company, USA, and Acros Chemical Company, USA, and used without further purification unless otherwise mentioned. The melting point was determined by an electro-thermal IA9000 series digital melting point apparatus and is uncorrected. Microanalyses were carried out using a Perkin-Elmer 2400II elemental analyzer. Infrared (IR) spectra and solution electronic spectra were recorded on Nicolet Magna IR (Series II) and Shimadzu UV-160A spectrophotometers, respectively. <sup>1</sup>H NMR spectra and electro-spray ionization mass (ESI-MS) measurements were made using a Bruker Advance 400 MHz and Finnigan LCQ Decapx MAX mass spectrometer, respectively.

### 2.2. Synthesis of the title compound **1**

The compound **1** has been synthesized by following a reported procedure [25]. Bis(4-aminophenyl)methane (1 mmol) was dissolved in 30 mL of dehydrated methanol, and 2-hydroxybenzaldehyde (2 mmol) was added drop-wise over 10 min. The reaction mixture was refluxed for 4 h at 70 °C, maintaining dry condition. A yellow precipitate was filtered and washed several times with *n*-hexane and then re-crystallized from methanol and dried in vacuum to obtain the pure yellow solid. Single crystals suitable for analysis were obtained by the slow evaporation of methanolic solution (Scheme 1).

2, 2'-(((Methylene-bis(4, 1-phenylene))bis(azanylylidene))bis(methanylylidene))diphenol: Color: Yellow. Yield: 85%. FT-IR (KBr, ν, cm<sup>-1</sup>): 1617, 1595, 1563. <sup>1</sup>H-NMR (400 MHz, CDCl<sub>3</sub>, δ, ppm): 13.28 (bs, 2H, OH), 8.65 (s, 2H, =CH), 7.41 (m, J = 7.3 Hz,

4H, Ar-H), 7.26 (m, 8H, Ar-H), 7.04 (d, J = 7.8 Hz, 2H, Ar-H), 6.96 (t, J = 7.8 Hz, 2H, Ar-H), 4.07 (s, 2H, CH<sub>2</sub>). ESI-MS (*m/z*, %): 407.39 (LH<sub>2</sub><sup>+</sup>, 100%). Anal. calcd. for C<sub>27</sub>H<sub>22</sub>N<sub>2</sub>O<sub>2</sub>: C, 79.78; H, 5.46; N, 6.89. Found: C, 79.62; H, 5.43; N, 6.97%. UV-Vis (MeOH, λ<sub>max</sub>, nm): 330, 280.

### 2.3. X-ray crystallography

Single crystal X-ray data of compound **1** was collected using MoKα (λ = 0.71073 Å) radiation on a Bruker APEX II diffractometer equipped with CCD area detector. The crystal was kept at 100 K during data collection. Using Olex2 [26], the structure was solved with the SHELXS [27] structure solution program using Direct Methods and refined with the SHELXL [28] refinement package using Least Squares minimization. Atoms other than hydrogen atoms were treated anisotropically. The hydrogen atoms were geometrically fixed. The crystallographic details of compound **1** are summarized in Table 1, the bond lengths, bond angles and torsion angles of compound **1** are listed in Tables 2-4, respectively.

### 2.4. Theoretical calculations

Gaussian 09 program [29] has been used for the quantum chemical calculations. The possible ground state structures have been optimized with density functional theory (DFT) at B3LYP/6-311G\*\*. GaussView 5 program [30] was used for the visualization of the studied systems.

### 2.5. Hirshfeld Surface Calculations

For obtaining additional insight into the intermolecular interaction of molecular crystals, Hirshfeld surface analysis helps as a powerful set-up.

**Table 2.** Bond lengths for the title compound.

Atom	Atom	Length (Å)	Atom	Atom	Length (Å)
N1	C8	1.4139(19)	C11	C14	1.513(2)
N1	C7	1.2793(19)	C11	C12	1.382(2)
O1	C5	1.344(2)	C5	C6	1.387(2)
C8	C13	1.379(2)	C10	C9	1.382(2)
C8	C9	1.388(2)	C13	C12	1.379(2)
C4	C7	1.445(2)	C3	C2	1.372(2)
C4	C5	1.399(2)	C2	C1	1.375(3)
C4	C3	1.391(2)	C6	C1	1.372(3)
C11	C10	1.376(2)			

**Table 3.** Bond angles for the title compound.

Atom	Atom	Atom	Angle (°)	Atom	Atom	Atom	Angle (°)
C7	N1	C8	121.43(13)	O1	C5	C6	119.46(16)
C13	C8	N1	117.09(13)	C6	C5	C4	119.45(16)
C13	C8	C9	118.02(14)	C11	C10	C9	122.02(15)
C9	C8	N1	124.88(14)	C12	C13	C8	121.11(15)
C5	C4	C7	121.40(14)	C10	C9	C8	120.16(15)
C3	C4	C7	120.01(14)	C2	C3	C4	121.51(17)
C3	C4	C5	118.59(15)	C11 <sup>1</sup>	C14	C11	109.79(18)
N1	C7	C4	122.28(14)	C13	C12	C11	121.30(15)
C10	C11	C14	121.49(13)	C3	C2	C1	119.27(17)
C10	C11	C12	117.31(14)	C1	C6	C5	120.46(18)
C12	C11	C14	121.11(13)	C6	C1	C2	120.71(17)
O1	C5	C4	121.09(15)				

<sup>1</sup>1-x, +y, 3/2-z.**Table 4.** Torsion angles for the title compound.

A	B	C	D	Angle (°)	A	B	C	D	Angle (°)
N1	C8	C13	C12	178.34(14)	C5	C4	C3	C2	1.3(2)
N1	C8	C9	C10	-179.75(14)	C5	C6	C1	C2	0.1(3)
O1	C5	C6	C1	-179.61(17)	C10	C11	C14	C11 <sup>1</sup>	-93.61(15)
C8	N1	C7	C4	179.78(12)	C10	C11	C12	C13	0.8(2)
C8	C13	C12	C11	1.7(2)	C13	C8	C9	C10	1.5(2)
C4	C5	C6	C1	0.6(3)	C9	C8	C13	C12	-2.8(2)
C4	C3	C2	C1	-0.5(3)	C3	C4	C7	N1	178.71(15)
C7	N1	C8	C13	-166.32(14)	C3	C4	C5	O1	178.93(15)
C7	N1	C8	C9	14.9(2)	C3	C4	C5	C6	-1.3(2)
C7	C4	C5	O1	-0.3(2)	C3	C2	C1	C6	-0.2(3)
C7	C4	C5	C6	179.52(15)	C14	C11	C10	C9	174.60(15)
C7	C4	C3	C2	-179.53(14)	C14	C11	C12	C13	-175.94(15)
C11	C10	C9	C8	1.0(2)	C12	C11	C10	C9	-2.1(2)
C5	C4	C7	N1	-2.1(2)	C12	C11	C14	C11 <sup>1</sup>	82.95(14)

<sup>1</sup>1-x, +y, 3/2-z.

The size and shape of Hirshfeld surface allow the qualitative and quantitative study and imagining of intermolecular close contacts in molecular crystals [31]. The Hirshfeld surface enclosing a molecule is defined by a set of points in 3D space where the contribution to the electron density from the molecule of interest is equal to the contribution from all other molecules. Molecular Hirshfeld surfaces are built based on electron distribution calculated as the sum of spherical atom electron densities [32,33]. The identification of the regions of particular importance to intermolecular interactions is achieved by mapping normalized contact distance ( $d_{\text{norm}}$ ), expressed as:  $d_{\text{norm}} = (d_i - r_i^{\text{vdw}}) / r_i^{\text{vdw}} + (d_e - r_e^{\text{vdw}}) / r_e^{\text{vdw}}$ ; where  $r_i^{\text{vdw}}$  and  $r_e^{\text{vdw}}$  are the van der Waals radii of the atoms [34]. The value of  $d_{\text{norm}}$  is negative or positive when intermolecular contacts are shorter or longer than  $r^{\text{vdw}}$ , respectively. Due to the symmetry between  $d_e$  and  $d_i$  in the expression for  $d_{\text{norm}}$ , where two Hirshfeld surfaces touch, both will display a red spot identical in color intensity as well as size and shape [35]. The mixture of  $d_e$  and  $d_i$  in the form of a 2D fingerprint plot provides a summary of intermolecular contacts in the crystal and are in complement to the Hirshfeld surfaces [34]. The information about the intermolecular interactions in the immediate environment of each molecule in the asymmetric unit is achieved by such plots. In addition, the close contacts between particular atom types can be highlighted in so-called resolved fingerprint plots [36], which allow the facile assignment of an intermolecular contact to a certain type of interaction and quantitatively summarize the nature and type of intermolecular contacts. Two additional colored properties (shape index and

curvedness) based on the local curvature of the surface can also be specified [37]. The Hirshfeld surfaces are mapped with  $d_{\text{norm}}$ , shape-index, curvedness and 2D fingerprint plots (full and resolved) reported in this manuscript were generated using Crystal-Explorer 3.1 [38].

## 2.6. Molecular electrostatic potential

The molecular electrostatic potential at a given point around a molecule can be defined in terms of total charge distribution of the molecule and related with the dipole moments. It supplies a method to understand the electron density which is useful for determining the electrophilic reactivity and nucleophilic reactivity along with hydrogen-bonding interactions [39,40].

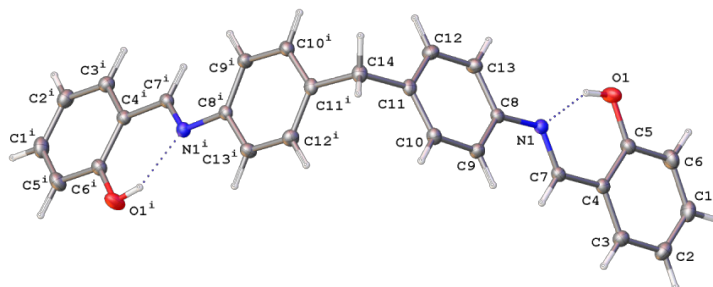
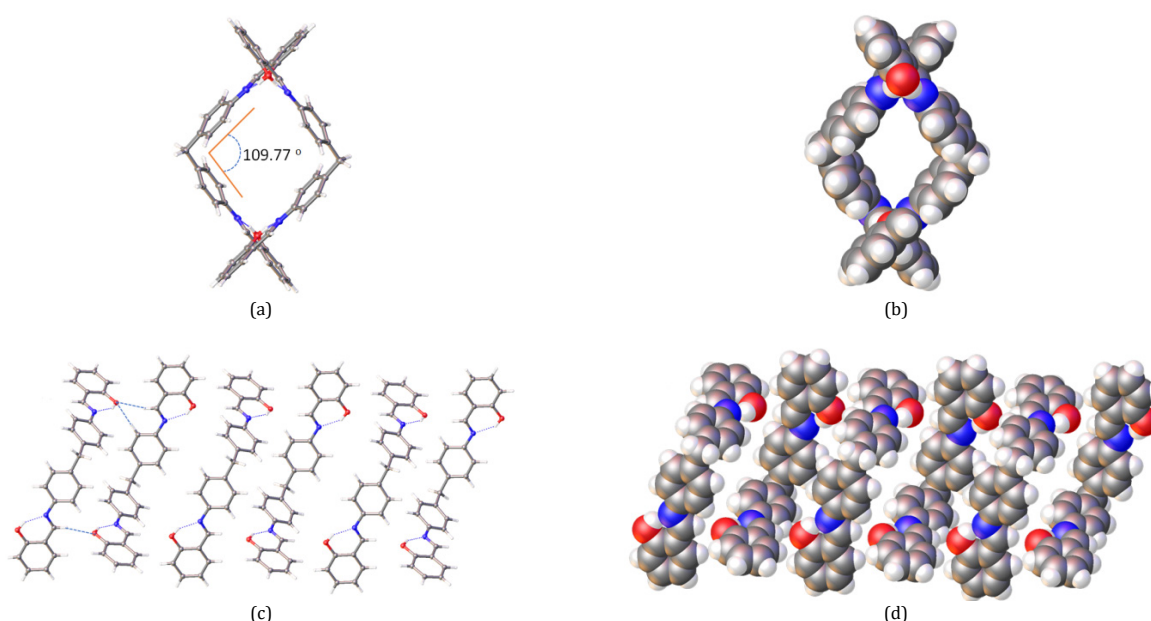
## 3. Results and discussion

### 3.1. Synthesis and structure

The compound **1** was synthesized in good yield and as yellow solid by condensing *bis*(4-aminophenyl)methane and 2-hydroxybenzaldehyde in 1:2 molar ratio in anhydrous methanol (Scheme 1). It crystallizes in monoclinic space group *C2/c* and the asymmetric unit contains a single molecule of compound **1**. The molecule of compound **1** has crystallographically imposed two-fold plain of symmetry. The ORTEP diagram of the compound **1** is shown in Figure 1.

**Table 5.** List of hydrogen bonding in compound **1**.

D	H	A	D-H (Å)	H...A (Å)	D-A (Å)	∠D-H...A (°)
C7	H7	O1	0.950	2.563	3.417	149.75
C9	H9	O1	0.950	3.279	4.070	141.97
C3	H3	O1	0.950	2.718	3.539	145.03
O1	H1	N1	0.840	1.841	2.589	147.81

**Figure 1.** The ORTEP diagram of the compound **1**. H-bondings are shown in dotted line.**Figure 2.** Crystal structure of compound **1**, (a, b) top view, (b, c) layer structure. H-bondings are shown in dotted line

The central methylene C atom (C14) of the diphenylmethane moiety is displaced from the aromatic ring planes. The molecule of compound **1** is angular V-shaped conformation, with atom C14 coinciding with a crystallographic two-fold axis. The two O-H groups are *trans* to each other. The angle between the two arms originating from central methylene C atom (C14) is 109.77° and the symmetry-related C1/C2/C3/C4/C5/C6 phenol ring is 78.87°. The C8/C9/C10/C11/C12/C13 phenyl ring is not coplanar with the C1/C2/C3/C4/C5/C6 phenol ring, the interplanar angle is 12.93°. The imino plane is almost coplanar with the phenol ring, it is, rather, twisted considerably out of the plane of the phenol ring of *bis*(4-aminophenyl) methane. The dihedral angle between the two unique phenyl rings is 177.68° while the dihedral angle between the two central phenyl rings is 93.73°. In the crystal structure of compound **1**, there exists two intramolecular O-H...N hydrogen bonds between the hydroxyl hydrogen and imino nitrogen atoms. Detailed information regarding hydrogen bonds in the molecules of compound **1** is given in Table 5. The packing of the molecules is shown in Figure 2. The molecules are stabilized by several weak non-covalent interactions including C-H...O bonds, and  $\pi$ - $\pi$  interactions resulting the formation of layered structure with direction of propagation of two adjacent layers

are in opposite direction. Each layer is stabilized by  $\pi$ - $\pi$  interactions. Top view of the structure formed rectangular channel (Figure 2a and b). There is a chance of *keto-enol* tautomerism in compound **1**, but the in the crystal structure of compound **1**, the molecule exists in the *enol* form.

### 3.2. Theoretical investigations

The optimized bond length and angles for the compound **1** is well replicated with the experimental single crystal X-ray diffraction structure data. The optimized structure of compound **1** has been shown in Figure 3. The surface plots of HOMO and LUMO of compound **1** have been depicted in Figure 4. The ground state energy of compound **1** achieved in DFT calculation is -1302.14 a.u. The HOMO-LUMO energy gap in compound **1** is 2.9639 eV.

### 3.3. Molecular Hirshfeld surfaces

The Hirshfeld surface is a suitable tool for describing the surface characteristics of molecules. The molecular Hirshfeld surface of compound **1** was generated using a standard (high) surface resolution with the 3D  $d_{\text{norm}}$  surfaces mapped over a fixed color scale of 0.22 (red) to 1.4 Å (blue).

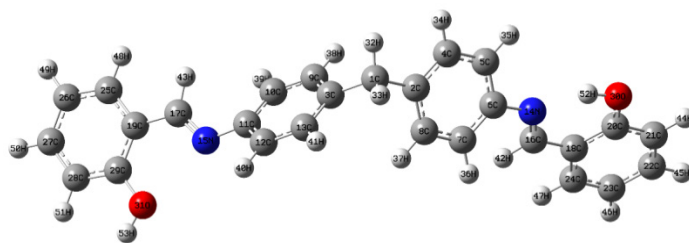


Figure 3. Optimized molecular structure of compound 1.

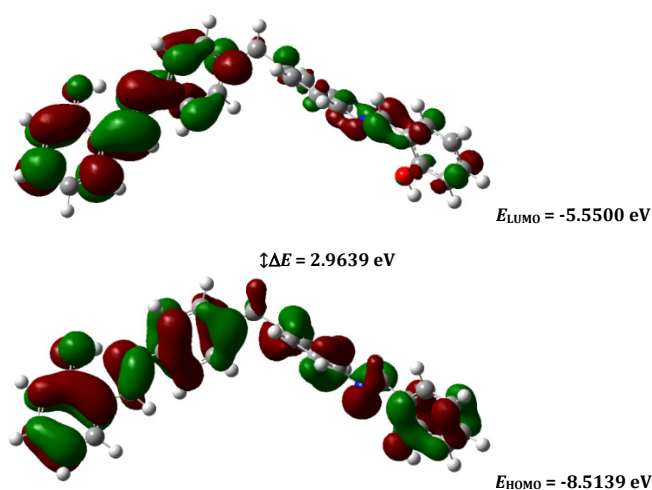
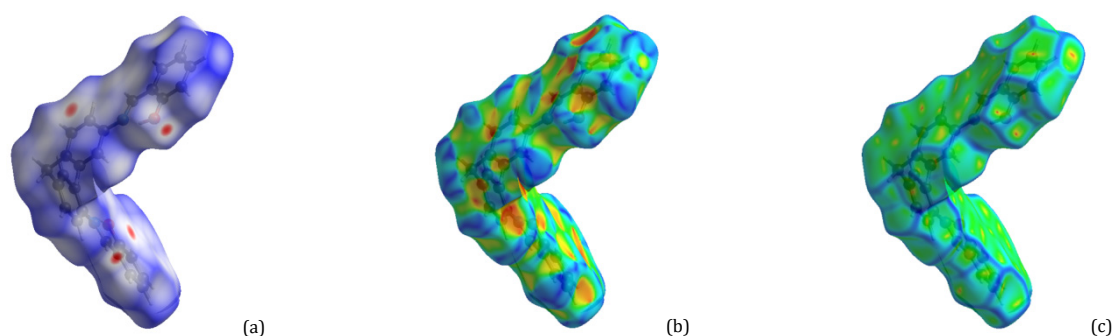


Figure 4. HOMO-LUMO energy levels and energy gap of the compound 1.

Figure 5. Hirshfeld surfaces of compound 1, (a) 3D  $d_{\text{norm}}$  surface, (b) shape index, and (c) curvedness.

The shape index mapped in the color range of -1.0 to 1.0, and curvedness was in the range of -4.0 to 0.4. The surfaces were shown to be transparent to allow visualization of the molecular moiety in a similar orientation for all of the structures around which they were calculated. The molecular Hirshfeld surfaces ( $d_{\text{norm}}$ , Shape index and curvedness) of compound 1 have been shown in Figure 5. The pattern of adjacent red and blue triangles that appears on the shape index surfaces of compound 1 and a relatively large and flat green region at the same side of the molecule on the corresponding curvedness surfaces, confirms the presence of  $\pi\cdots\pi$  interactions in compound 1.

The Hirshfeld surface analysis of compound 1 shows that  $\text{H}\cdots\text{H}$ ,  $\text{C}\cdots\text{H}$ , and  $\text{O}\cdots\text{H}$  interactions of 53.3, 13.2 and 5.4%, respectively, which revealed that the main intermolecular interactions were  $\text{H}\cdots\text{H}$  intermolecular interactions. Both the  $\text{C}\cdots\text{H}$  and  $\text{O}\cdots\text{H}$  interactions were represented by a small area in the right side of the top in the 2D fingerprint map, whereas the  $\text{H}\cdots\text{H}$  interactions were represented by the largest in the fingerprint plot (Figure 6) and thus, had the most significant contribution to the total Hirshfeld surfaces (53.3%).

### 3.4. Molecular electrostatic potential

Molecular electrostatic potential can simultaneously display molecular size, shape as well as positive, negative and neutral electrostatic potential regions in terms of color grading. The order of the electrostatic potential is as follows: Red < orange < yellow < green < blue. Negative regions of molecular electrostatic potential are rich in electrons and are focused on electronegative atoms. Positive regions are electrons deficient and these sites are mainly around hydrogen atoms. Molecular electrostatic potential of compound 1 has been shown in Figure 7.

### 4. Conclusion

In conclusion, we have reported here the synthesis, crystal structure and Hirshfeld surface analysis of a di-Schiff base ligand, 2,2'-(((methylene-bis(4,1-phenylene))bis(azanylylidene))bis(methanylylidene))diphenol (1), which is a building block of several metal helicates.

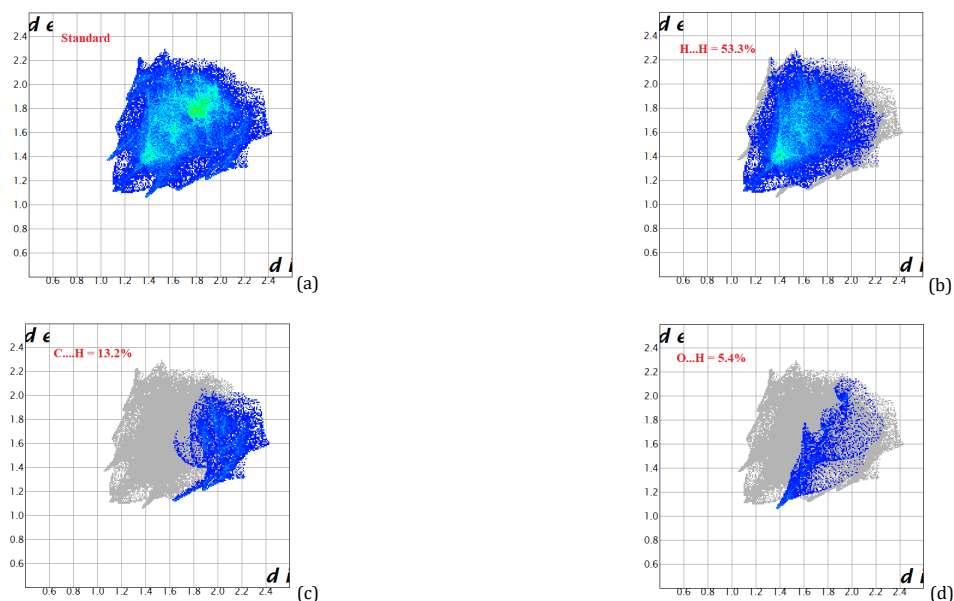


**Figure 6.** 2D Fingerprint plots of compound **1**, (a) standard full, (b) resolved into H...H, (c) resolved into C...H, and (d) O...H contacts, showing the percentages of contacts contributing to the total Hirshfeld surface area of the molecule.

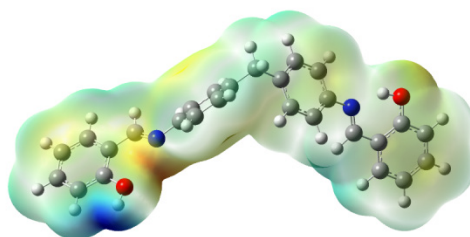


**Figure 7.** Molecular electrostatic potential of compound **1**.

Interestingly, this molecule has an angular shape with intramolecular and intermolecular hydrogen bonding. In crystal structure, the molecule exists in the *enol* form and is located on a two-fold axis of symmetry; where the central methylene carbon atom of the diphenylmethane moiety is displaced from the aromatic ring planes. The Hirshfeld surface analysis of compound **1** shows that H...H, C...H, and O...H interactions of 53.3, 13.2, and 5.4%; respectively, which exposed that the main intermolecular interactions were H...H intermolecular interactions.

### Acknowledgements

Goutam Kumar Patra would like to thank the Department of Science and Technology (SR/FST/CSI-264/2014 and EMR/2017/0001789) and Department of Biotechnology, Government of India, New Delhi for financial support.

### Supporting information

CCDC-2101426 contains the supplementary crystallographic data for this paper. These data can be obtained free of charge via <https://www.ccdc.cam.ac.uk/structures/>, or by e-mailing [data\\_request@ccdc.cam.ac.uk](mailto:data_request@ccdc.cam.ac.uk), or by contacting The Cambridge Crystallographic Data Centre, 12 Union Road, Cambridge CB2 1EZ, UK; fax: +44(0)1223-336033.

### Disclosure statement

Conflict of interests: The authors declare that they have no conflict of interest. Ethical approval: All ethical guidelines have been adhered. Sample availability: Sample of the compound **1** is available from the author.

### CRediT authorship contribution statement

Conceptualization: Goutam Kumar Patra; Methodology: Goutam Kumar Patra; Software: Dinesh De; Validation: Goutam Kumar Patra; Formal Analysis: Goutam Kumar Patra; Investigation: Goutam Kumar Patra; Resources: Goutam Kumar Patra; Data Curation: Dinesh De Writing - Original Draft: Goutam Kumar Patra; Writing - Review and Editing: Dinesh De; Visualization: Dinesh De; Funding acquisition: Goutam Kumar Patra; Supervision: Goutam Kumar Patra; Project Administration: Goutam Kumar Patra.

### ORCID and Email

Goutam Kumar Patra

 [goutam.patra@ggu.ac.in](mailto:goutam.patra@ggu.ac.in)

 <https://orcid.org/0000-0003-3151-0284>

Dinesh De

 [d2chem@gmail.com](mailto:d2chem@gmail.com)

 <https://orcid.org/0000-0001-7850-8718>

### References

- [1]. Dey, S.; Sen, C.; Sinha, C. Chromogenic Hydrazone Schiff Base Reagent: Spectrophotometric Determination of CN<sup>-</sup> Ion. *Spectrochim. Acta A Mol. Biomol. Spectrosc.* **2020**, *225* (117471), 117471.
- [2]. Sztanke, K.; Maziarka, A.; Osinka, A.; Sztanke, M. An Insight into Synthetic Schiff Bases Revealing Antiproliferative Activities in Vitro. *Bioorg. Med. Chem.* **2013**, *21* (13), 3648–3666.
- [3]. Chandra, R.; Manna, A. K.; Sahu, M.; Rout, K.; Patra, G. K. Simple Salicylaldehyde-Functionalized Dipodal Bis Schiff Base Chromogenic and Fluorogenic Chemosensors for Selective and Sensitive Detection of Al<sup>3+</sup> and Cr<sup>3+</sup>. *Inorganica Chim. Acta* **2020**, *499* (119192), 119192.
- [4]. Gupta, K. C.; Sutar, A. K. Catalytic Activities of Schiff Base Transition Metal Complexes. *Coord. Chem. Rev.* **2008**, *252* (12–14), 1420–1450.

- [5]. Burrows, C. J.; Muller, J. G.; Poulter, G. T.; Rokita, S. E. Nickel-Catalyzed Oxidations: From Hydrocarbons to DNA. *Acta Chem. Scand.* **1996**, *50* (4), 337–344.
- [6]. Pang, Y.; Cui, S.; Li, B.; Zhang, J.; Wang, Y.; Zhang, H. Metal-Dependent Assembly of a Helical-[Co3L3] Cluster versus a Meso-[Cu2L2] Cluster with O,N,N',O'-Schiff Base Ligand: Structures and Magnetic Properties. *Inorg. Chem.* **2008**, *47* (22), 10317–10324.
- [7]. Fouda, M. F. R.; Abd-Elzaher, M. M.; Shakdofa, M. M.; El-Saied, F. A.; Ayad, M. I.; El Tabl, A. S. Synthesis and Characterization of a Hydrazone Ligand Containing Antipyrine and Its Transition Metal Complexes. *J. Coord. Chem.* **2008**, *61* (12), 1983–1996.
- [8]. Boal, A. K.; Rosenzweig, A. C. Structural Biology of Copper Trafficking. *Chem. Rev.* **2009**, *109* (10), 4760–4779.
- [9]. Salah, B. A.; Kandil, A. T.; Abd El-Nasser, M. G. Synthesis, Characterization, Computational and Biological Activity of Novel Hydrazone Complexes. *J. Radiat. Res. Appl. Sci.* **2019**, *12* (1), 383–392.
- [10]. Kruger, P. E.; Martin, N.; Nieuwenhuyzen, M. Dinuclear Double Helicates with a Twist: Synthesis, Structure and Supramolecular Entanglement in [M2L2] Metallo-Helices [M = Co(II), Cu(II), H2L = Bis(N-Salicylidene-4,4'-Diaminodiphenyl)Methane]. *J. Chem. Soc.* **2001**, No. 13, 1966–1970.
- [11]. Ogawa, K.; Harada, J. Aggregation Controlled Proton Tautomerization in Salicylideneanilines. *J. Mol. Struct.* **2003**, *647* (1–3), 211–216.
- [12]. Vitale, M. Luminescent Mixed Ligand Copper(I) Clusters (Cu)n(L)m (L=pyridine, Piperidine): Thermodynamic Control of Molecular and Supramolecular Species. *Coord. Chem. Rev.* **2001**, *219–221*, 3–16.
- [13]. Constable, E. C.; Ward, M. D.; Tocher, D. A. Molecular Helicity in Inorganic Complexes; Bi- and Tri-Nuclear Complexes of 2,2':6',2'':6'', 2''':6'''-2''''-6''''-2'''''-Sexipyridine and the Crystal and Molecular Structure of Bis(μ-2,2':6',2'':6'', 2''':6'''-2''''-6''''-2'''''-Sexipyridine-K3N, N',N'':K3N''',N''',N''''') Dication Hexafluorophosphate-Acetonitrile (1/4). *J. Chem. Soc., Dalton Trans.* **1991**, No. 7, 1675–1683.
- [14]. Filarowski, A.; Koll, A.; Glowiak, T. Proton Transfer Equilibrium in the Intramolecular Hydrogen Bridge in Sterically Hindered Schiff Bases. *J. Mol. Struct.* **2002**, *615* (1–3), 97–108.
- [15]. Popović, Z.; Pavlović, G.; Matković-Čalogović, D.; Roje, V.; Leban, I. On Tautomerism of Two 5-Methoxysalicylaldehyde Structural Isomers in the Solid State: Structural Study of N-(o-Hydroxyphenyl)-5-Methoxy salicylaldehyde and N-(m-Hydroxyphenyl)-5-Methoxysalicylaldehyde. *J. Mol. Struct.* **2002**, *615* (1–3), 23–31.
- [16]. Liu, A.; Yang, L.; Zhang, Z.; Zhang, Z.; Xu, D. A Novel Rhodamine-Based Colorimetric and Fluorescent Sensor for the Dual-Channel Detection of Cu<sup>2+</sup> and Fe<sup>3+</sup> in Aqueous Solutions. *Dyes Pigm.* **2013**, *99* (2), 472–479.
- [17]. Ghorai, A.; Mondal, J.; Chowdhury, S.; Patra, G. K. Solvent-Dependent Fluorescent-Colorimetric Probe for Dual Monitoring of Al<sup>3+</sup> and Cu<sup>2+</sup> in Aqueous Solution: An Application to Bio-Imaging. *Dalton Trans.* **2016**, *45* (28), 11540–11553.
- [18]. Mao, J.; Wang, L.; Dou, W.; Tang, X.; Yan, Y.; Liu, W. Tuning the Selectivity of Two Chemosensors to Fe(III) and Cr(III). *Org. Lett.* **2007**, *9* (22), 4567–4570.
- [19]. Yoshida, N.; Ichikawa, K. Synthesis and Structure of a Dinuclear Zinc(II) Triple Helix of an N,N-Bis-Bidentate Schiff Base: New Building Blocks for the Construction of Helical Structures. *Chem. Commun. (Camb.)* **1997**, No. 12, 1091–1092.
- [20]. Rout, K.; Manna, A. K.; Sahu, M.; Mondal, J.; Singh, S. K.; Patra, G. K. Triazole-Based Novel Bis Schiff Base Colorimetric and Fluorescent Turn-on Dual Chemosensor for Cu<sup>2+</sup> and Pb<sup>2+</sup>: Application to Living Cell Imaging and Molecular Logic Gates. *RSC Adv.* **2019**, *9* (44), 25919–25931.
- [21]. Manna, A. K.; Rout, K.; Chowdhury, S.; Patra, G. K. A Dual-Mode Highly Selective and Sensitive Schiff Base Chemosensor for Fluorescent Colorimetric Detection of Ni<sup>2+</sup> and Colorimetric Detection of Cu<sup>2+</sup>. *Photochem. Photobiol. Sci.* **2019**, *18* (6), 1512–1525.
- [22]. Sahu, M.; Kumar Manna, A.; Rout, K.; Mondal, J.; Patra, G. K. A Highly Selective Thiosemicarbazone Based Schiff Base Chemosensor for Colorimetric Detection of Cu<sup>2+</sup> and Ag<sup>+</sup> Ions and Turn-on Fluorometric Detection of Ag<sup>+</sup> Ions. *Inorganica Chim. Acta* **2020**, *508* (119633), 119633.
- [23]. Mishra, J.; Kaur, H.; Ganguli, A. K.; Kaur, N. Fluorescent Chemosensor Based on Urea/Thiourea Moiety for Sensing of Hg(II) Ions in an Aqueous Medium with High Sensitivity and Selectivity: A Comparative Account on Effect of Molecular Architecture on Chemosensing. *J. Mol. Struct.* **2018**, *1161*, 34–43.
- [24]. Rana, S.; Mittal, S. K.; Singh, N.; Singh, J.; Banks, C. E. Schiff Base Modified Screen Printed Electrode for Selective Determination of Aluminium(III) at Trace Level. *Sens. Actuators B Chem.* **2017**, *239*, 17–27.
- [25]. Yoshida, N.; Ichikawa, K.; Shiro, M. Supramolecular Motifs in Metal Complexes of Schiff Bases. Part 5. Zinc(II)-Assisted Self-Assembly of Some Bis-N,N- and N,O-Bidentate Schiff Bases and Chiral Packing Modes in Solid State. *J. Chem. Soc., Perkin Trans. 2* **2000**, No. 1, 17–26.
- [26]. Dolomanov, O. V.; Bourhis, L. J.; Gildea, R. J.; Howard, J. A. K.; Puschmann, H. OLEX2: A Complete Structure Solution, Refinement and Analysis Program. *J. Appl. Crystallogr.* **2009**, *42* (2), 339–341.
- [27]. Sheldrick, G. M. A Short History of SHELX. *Acta Crystallogr. A* **2008**, *64* (1), 112–122.
- [28]. Sheldrick, G. M. Crystal Structure Refinement with SHELXL. *Acta Crystallogr. C Struct. Chem.* **2015**, *71* (Pt 1), 3–8.
- [29]. Frisch, M. J.; Trucks, G. W.; Schlegel, H. B.; Scuseria, G. E.; Robb, M. A.; Cheeseman, J. R.; Scalmani, G.; Barone, V.; Mennucci, B.; Petersson, G. A.; Nakatsuji, H.; Caricato, M.; Li, X.; Hratchian, H. P.; Izmaylov, A. F.; Bloino, J.; Zheng, G.; Sonnenberg, J. L.; Hada, M.; Ehara, M.; Toyota, K.; Fukuda, R.; Hasegawa, J.; Ishida, M.; Nakajima, T.; Honda, Y.; Kitao, O.; Nakai, H.; Vreven, T.; Montgomery, J. A.; Peralta, J. E.; Ogliaro, F.; Bearpark, M.; Heyd, J. J.; Brothers, E.; Kudin, K. N.; Staroverov, V. N.; Kobayashi, R.; Normand, J.; Raghavachari, K.; Rendell, A.; Burant, J. C.; Iyengar, S. S.; Tomasi, J.; Cossi, M.; Rega, N.; Millam, J. M.; Klene, M.; Knox, J. E.; Cross, J. B.; Bakken, V.; Adamo, C.; Jaramillo, J.; Gomperts, R.; Stratmann, R. E.; Yazyev, O.; A. J. Austin, A. J.; Cammi, R.; Pomelli, C.; Ochterski, J. W.; Martin, R. L.; Morokuma, K.; Zakrzewski, V. G.; Voth, G. A.; Salvador, P.; Dannenberg, J. J.; Dapprich, S.; Daniels, A. D.; Farkas, O.; Foresman, J. B.; Ortiz, J. V.; Cioslowski, J.; Fox, D. J. Gaussian, Inc., Gaussian 09, Revision A.02, Wallingford CT, 2009.
- [30]. Dennington, R.; Keith, T.; Millam, J.; Gaussview. Version 5; Semichem Inc: Shawnee Mission, KS, 2009.
- [31]. Norret, M.; Makha, M.; Sobolev, A. N.; Raston, C. L. Controlling the Confinement of Fullerene C60 Molecules Using a Saddle Shape Ni(II) Macrocycle. *New J Chem* **2008**, *32* (5), 808–812.
- [32]. Spackman, M. A.; McKinnon, J. J. Fingerprinting Intermolecular Interactions in Molecular Crystals. *CrystEngComm* **2002**, *4* (66), 378–392.
- [33]. Meng, X. X. Applications of Hirshfeld surfaces to ionic and mineral crystals, Ph.D. Thesis, University of New England, 2004.
- [34]. Pendás, A. M.; Luaña, V.; Pueyo, L.; Francisco, E.; Mori-Sánchez, P. Hirshfeld Surfaces as Approximations to Interatomic Surfaces. *J. Chem. Phys.* **2002**, *117* (3), 1017–1023.
- [35]. Hyde, S.; Ninham, B. W.; Andersson, S.; Larsson, K.; Landh, T.; Blum, Z.; Lidin, S. In *The Language of Shape*; Elsevier, 1997.
- [36]. Nishikawa, M.; Nomoto, K.; Kume, S.; Inoue, K.; Sakai, M.; Fujii, M.; Nishihara, H. Dual Emission Caused by Ring Inversion Isomerization of a 4-Methyl-2-Pyridyl-Pyrimidine Copper(I) Complex. *J. Am. Chem. Soc.* **2010**, *132* (28), 9579–9581.
- [37]. Desiraju, G. R. Crystal Engineering: A Holistic View. *Angew. Chem. Int. Ed Engl.* **2007**, *46* (44), 8342–8356.
- [38]. Spackman, P. R.; Turner, M. J.; McKinnon, J. J.; Wolff, S. K.; Grimwood, D. J.; Jayatilaka, D.; Spackman, M. A. CrystalExplorer: A Program for Hirshfeld Surface Analysis, Visualization and Quantitative Analysis of Molecular Crystals. *J. Appl. Crystallogr.* **2021**, *54* (Pt 3), 1006–1011.
- [39]. Sebastian, S.; Sundaraganesan, N. The Spectroscopic (FT-IR, FT-IR Gas Phase, FT-Raman and UV) and NBO Analysis of 4-Hydroxypiperidine by Density Functional Method. *Spectrochim. Acta A Mol. Biomol. Spectrosc.* **2010**, *75* (3), 941–952.
- [40]. Luque, F. J.; López, J. M.; Orozco, M. Perspective on “Electrostatic Interactions of a Solute with a Continuum. A Direct Utilization of Ab Initio Molecular Potentials for the Prediction of Solvent Effects.” *Theor. Chem. Acc.* **2000**, *103* (3–4), 343–345.



Copyright © 2022 by Authors. This work is published and licensed by Atlanta Publishing House LLC, Atlanta, GA, USA. The full terms of this license are available at <http://www.eurjchem.com/index.php/eurjchem/pages/view/terms> and incorporate the Creative Commons Attribution-Non Commercial (CC BY NC) (International, v4.0) License (<http://creativecommons.org/licenses/by-nc/4.0>). By accessing the work, you hereby accept the Terms. This is an open access article distributed under the terms and conditions of the CC BY NC License, which permits unrestricted non-commercial use, distribution, and reproduction in any medium, provided the original work is properly cited without any further permission from Atlanta Publishing House LLC (European Journal of Chemistry). No use, distribution or reproduction is permitted which does not comply with these terms. Permissions for commercial use of this work beyond the scope of the License (<http://www.eurjchem.com/index.php/eurjchem/pages/view/terms>) are administered by Atlanta Publishing House LLC (European Journal of Chemistry).